Mechanism Analysis of Modal Resonance in Converter-based Power Systems

Xianyu Zhou, Siqi Bu, *Senior Member, IEEE*

***Abstract*—The increasing integration of renewable energy and power electronics has brought various oscillation issues due to open-loop modal resonance, while the essential mechanism of open-loop modal resonance has not been fully discovered yet. In this connection, this paper firstly proposes the concept of participation factor transition (PFT), revealing the existence of PFT in open-loop modal interactions and the necessity of untraceable PFT in modal resonance. Secondly, participation factor transition analysis (PFT analysis) is conducted to investigate the contribution of PFT to modal interactions. Two categories of the PFT phenomenon, named participation factor conservation law (PFCL) and borrowing participation factor law (BPFL), are proposed to explain the essential mechanism of modal interactions in power systems. Participation factor transition index (PFTI) is proposed to determine whether PFT is traceable and then identify the dominant state variables that affect the modal interactions. Additionally, participation factor transition control (PFT control) is proposed to solve the modal resonance based on PFT analysis. Finally, the proposed participation factor transition analysis and control (PFTAC) are validated in two converter-based power systems, which not only verifies the critical role of PFT in modal interactions but also improves the small-signal stability of the power system.**

***Index Terms*—Participation factor conservation law (PFCL), borrowing participation factor law (BPFL), dominant factors of PFT, modal interactions.**

I. Introduction

With the continuous increase of renewable energy sources, the power system suffers from a series of stability issues, such as modal resonance when the converter is connected to a weak power grid [1]. To avoid threatening the security caused by modal resonance [2], it is of great significance to study the mechanism of modal resonance in the converter-based power systems [3]-[5].

Numerous research efforts have used the open-loop model to analyze the modal resonance in the power system. The system can be modeled by using two open-loop models for analysis, and each model represents a part of the power system. The power system can be formed by integrating the two sub-models, and the formation of the two subsystems is called the closed-loop model. The modes associated with these two open-loop models are called open-loop modes. Open-loop modes can interact with each other to form closed-loop modes when the two open-loop models are integrated, which is called modal interactions. When two concerned open-loop modes are closest to each other, modal interaction will turn to modal resonance [6] and [7]. Therefore, understanding the interaction mechanism between open-loop modes is essential. Different types of modal interaction mechanisms are analyzed in [6]–[10]. Residues are used in [8] and [9] to prove the open-loop modal resonance when the two open-loop modes are the closest. The modal resonance between the open-loop PMSG mode and the open-loop power system mode is investigated in [10] and [11] by applying damping torque analysis [12].

In addition to using the open-loop model to analyze modal resonance, general modal resonance is proposed in [13], extending the classification of traditional modal resonance with open-loop modal resonance, modal instability[14], and participation factors instability[15]. In the traditional modal resonance, Dobson introduces that near strong modal resonance and near weak modal resonance are caused by two closely spaced modes. However, modal resonance being strong or weak is a phenomenon, not a method for analyzing modal resonance. When two open-loop modes are close to each other and result in strong resonance, it can be regarded as near strong modal resonance. When two open-loop modes are close to each other while resulting in no obvious resonance, it can be regarded as near weak modal resonance. And it only focuses on two modes. However, modal resonance results from the interaction of multiple modes, rather than just two modes, as discovered in this paper. For modal instability/participation factors instability, they mentioned multiple modes, while the concept of "multiple modes" in this method refers to the change of participation of state variables in multiple modes. The approach is a tool to demonstrate modal analysis before and after parameter perturbations and explains the relationship between modes and participation factors while not revealing the interaction of modes. And they did not investigate the modal interaction caused by the parameter perturbation, which cannot properly study the modal resonance. In these references, a significant change of participation factors (PFs) has been observed either under a parameter perturbation or during the modal resonance. However, the change of PFs has not been carefully investigated, which may be the essential mechanism of modal resonance and thus is worth further study.

This work was supported in part by the National Natural Science Foundation of China for the Research Project under Grant 52077188, and in part by the Hong Kong Research Grant Council for the Research Project under Grants 15205424. (*Corresponding author: Siqi Bu.*)

Xianyu Zhou is with the Department of Electrical and Electronic Engineering, The Hong Kong Polytechnic University, Kowloon, Hong Kong, China. (e-mail: 21039266R@connect.polyu.hk).

Siqi Bu is with Department of Electrical and Electronic Engineering, Shenzhen Research Institute, Research Centre for Grid Modernisation, International Centre of Urban Energy Nexus, Centre for Advances in Reliability and Safety, Research Institute for Smart Energy, and Policy Research Centre for Innovation and Technology, The Hong Kong Polytechnic University, Kowloon, Hong Kong. (e-mail: siqi.bu@polyu.edu.hk).

Existing research has acknowledged the significance of PFs. Some new findings on PFs are uncovered in [16], presenting a previously unknown method that reveals the complex nature of PFs. The application of PFs is explored in the modal voltage stability analysis of multi-infeed high-voltage direct current (HVDC) systems, demonstrating their effectiveness in assessing the impact of HVDC converters on voltage stability and providing valuable insights for system design and operation [17]. Imperialist Competitive Algorithm (ICA) and PFs are combined to tune and determine the placement of PSS to improve the stability of the South Sulawesi power system [18]. However, PF in these references is mainly used to identify the state variables that significantly affect a given mode, and the exact relationship between relevant system parameters and concerned mode or modal interactions cannot be accurately quantified using PF.

Considering the above points, the mechanism of modal interactions has been systematically investigated in this paper by carefully studying the phenomena of participation factor transition (PFT). The important relationship of PFT and modal interactions is effectively revealed. The main contributions of this paper are:

1) The concept of PFT is proposed to quantitatively prove that the interaction of two open-loop modes is essentially caused by PFT, which is also the essential mechanism of modal resonance.

2) Participation factor transition analysis (PFT analysis) is proposed to systematically investigate the detailed PFT process in modal interactions. Two categories of PFT phenomenon, named participation factor conservation law (PFCL) and borrowing participation factor law (BPFL), have been established in PFT analysis to explain the formation of modal interaction via PFT explicitly. The proposed BPFL indicates that the modal resonance is among multiple modes and is caused by the untraceable PFT for the first time. However, previous studies only focus on two concerned modes to investigate the modal resonance and might not be able to identify the real dominant state variables of PFT associated with the rest of the modes.

3) Participation factor transition index (PFTI) is proposed as a criterion to determine whether PFT is traceable and to efficiently identify the associated key state variables of modal interactions. In previous studies, the key state variables are determined by the dominant PFs. However, in this paper, the key state variables are determined by the dominant PFT, which has been proven to be the intrinsic factor of modal resonance.

4) Participation factor transition control (PFT control) is proposed to fundamentally solve the modal resonance based on PFT analysis and PFTI effectively.

The remainder of this paper is organized as follows. Section II proposes the concept of PFT. Section III proposes PFT analysis with two defined categories of PFT phenomenon. Additionally, PFTI is proposed to identify the dominant state variables of the modal interactions, and PFT control is proposed to solve the modal resonance. Section IV gives two study cases to verify PFTAC. Finally, Section V concludes the paper.

II. Revealing the Key Role of Participation Factor Transition in Modal Interactions

A wind farm is connected to the power system as an example. Denote one of the wind turbines as the "wind turbine subsystem", and the rest of the power system including other wind turbines, as the "power system subsystem". Appendix A derives the open-loop state space model.

The closed-loop model is established by combining the two open-loop subsystem models,

$$\Delta\dot{\boldsymbol{X}}_c = \hat{\boldsymbol{A}}_c \Delta\boldsymbol{X}_c \tag{1}$$

where $\boldsymbol{X}_c$ is the vector composed of all state variables of the power system, and $\hat{\boldsymbol{A}}_c$ is the corresponding state space matrix of the power system.

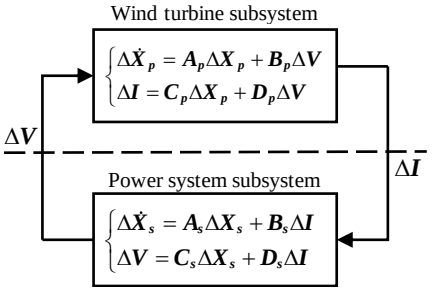

Fig. 1. Closed-loop system model by combining two open-loop subsystem models.

According to the mathematical properties of the eigenvalues, for a real matrix $\boldsymbol{A}$, if there are complex eigenvalues, they must appear in conjugate pairs. Therefore, the sum of the eigenvalues of the matrix is equal to the sum of the real parts of the eigenvalues, and it is also equal to the sum of the diagonal elements of the matrix $\boldsymbol{A}$ [20]. Since the real part of the eigenvalue reflects the damping of the system, the sum of all the eigenvalues of the system can be regarded as the total damping of the system [21].

For an open-loop mode,

$$\begin{aligned}
\lambda_i &= \boldsymbol{w}_i^T \boldsymbol{A} \boldsymbol{v}_i \\
&= \begin{bmatrix} \boldsymbol{w}_{i1}^T & \boldsymbol{w}_{i2}^T \cdots \boldsymbol{w}_{in}^T \end{bmatrix} \begin{bmatrix} a_{11} & a_{12} \cdots a_{1n} \\ a_{21} & a_{22} \cdots a_{2n} \\ \vdots & \ddots & \vdots \\ a_{n1} & a_{n2} \cdots a_{nn} \end{bmatrix} \begin{bmatrix} \boldsymbol{v}_{1i} \\ \boldsymbol{v}_{2i} \\ \vdots \\ \boldsymbol{v}_{ni} \end{bmatrix} \\
&= (\sum_{j=1}^{n} \boldsymbol{w}_{ij}^T a_{j1}) \boldsymbol{v}_{1i} + (\sum_{j=1}^{n} \boldsymbol{w}_{ij}^T a_{j2}) \boldsymbol{v}_{2i} + \cdots + (\sum_{j=1}^{n} \boldsymbol{w}_{ij}^T a_{jn}) \boldsymbol{v}_{ni} \\
&= \sum_{k=1}^{n} \boldsymbol{w}_{ki} \boldsymbol{v}_{ki} a_{kk} + \sum_{k=1}^{n} \sum_{j=1, j\neq k}^{n} \boldsymbol{w}_{ji} \boldsymbol{v}_{ki} a_{jk}
\end{aligned} \tag{2}$$

The closed-loop mode $\hat{\lambda}_i$ is similar to the open-loop mode,

$$\hat{\lambda}_i = \sum_{k=1}^{n} \hat{\boldsymbol{w}}_{ki} \hat{\boldsymbol{v}}_{ki} \hat{a}_{kk} + \sum_{k=1}^{n} \sum_{\substack{j=1 \\ j\neq k}}^{n} \hat{\boldsymbol{w}}_{ji} \hat{\boldsymbol{v}}_{ki} \hat{a}_{jk} \tag{3}$$

Modal interactions are defined as the difference between the closed-loop mode and open-loop mode[6], [7]. Subtract equation (2) from (3) yields (4) as follows,

$$\begin{aligned}\Delta\lambda_i &= \hat{\lambda}_i - \lambda_i \\ &= \sum_{k=1}^{n}(\hat{\boldsymbol{w}}_{ki}\hat{\boldsymbol{v}}_{ki}\hat{a}_{kk} - \boldsymbol{w}_{ki}\boldsymbol{v}_{ki}a_{kk}) \\ &+\sum_{k=1}^{n}\sum_{\substack{j=1\\ j\neq k}}^{n}\hat{\boldsymbol{w}}_{ji}\hat{\boldsymbol{v}}_{ki}\hat{a}_{jk} - \sum_{k=1}^{n}\sum_{\substack{j=1\\ j\neq k}}^{n}\boldsymbol{w}_{ji}\boldsymbol{v}_{ki}a_{jk} \\ &= \sum_{k=1}^{n}[(\hat{\boldsymbol{w}}_{ki}\hat{\boldsymbol{v}}_{ki} - \boldsymbol{w}_{ki}\boldsymbol{v}_{ki})\hat{a}_{kk} + \boldsymbol{w}_{ki}\boldsymbol{v}_{ki}(\hat{a}_{kk} - a_{kk})] \\ &+\sum_{k=1}^{n}\sum_{\substack{j=1\\ j\neq k}}^{n}\hat{\boldsymbol{w}}_{ji}\hat{\boldsymbol{v}}_{ki}\hat{a}_{jk} - \sum_{k=1}^{n}\sum_{\substack{j=1\\ j\neq k}}^{n}\boldsymbol{w}_{ji}\boldsymbol{v}_{ki}a_{jk}\end{aligned} \tag{4}$$

Assume the following equations,

$$\Delta p_{ki} = \hat{\boldsymbol{w}}_{ki}\hat{\boldsymbol{v}}_{ki} - \boldsymbol{w}_{ki}\boldsymbol{v}_{ki} \tag{5}$$

$$\Delta a_{kk} = \hat{a}_{kk} - a_{kk} \tag{6}$$

$$F_{1i} = \sum\nolimits_{k=1}^{n}\sum\nolimits_{j=1,\, j\neq k}^{n}\boldsymbol{w}_{ji}\boldsymbol{v}_{ki}a_{jk} \tag{7}$$

$$F_{2i} = \sum\nolimits_{k=1}^{n}\sum\nolimits_{j=1,\, j\neq k}^{n}\hat{\boldsymbol{w}}_{ji}\hat{\boldsymbol{v}}_{ki}\hat{a}_{jk} \tag{8}$$

$$\Delta F_i = F_{2i} - F_{1i} \tag{9}$$

Substituting equations (5)-(9) into equation (4),

$$\Delta\lambda_i = \sum_{k=1}^{n}(\Delta p_{ki}\hat{a}_{kk} + \boldsymbol{w}_{ki}\boldsymbol{v}_{ki}\Delta a_{kk}) + \Delta F_i \tag{10}$$

The variation of the diagonal elements is Δa_{kk}. Based on the definition of PFs, $p_{ki} = \partial\lambda_i/\partial a_{kk}$, PFs are relevant to Δa_{kk}. The remaining part that is neither related to the PFs nor the diagonal elements is ΔF_i.

Definition: PFT is the transition of state variables in the mode. PFT_{ki} can be represented as $\Delta p_{ki}\hat{a}_{kk} + \boldsymbol{w}_{ki}\boldsymbol{v}_{ki}\Delta a_{kk}$ for the k^{th} state variable in the i^{th} mode, which is combined by PF variation Δp_{ki} and the diagonal elements Δa_{kk}.

The definition of PFT reveals the transition of PFs from the open-loop mode to the closed-loop mode. Based on the definition of PFT, modal interactions (10) can be simplified (11),

$$\Delta\lambda_i = \sum_{k=1}^{n} PFT_{ki} + \Delta F_i \tag{11}$$

III. Participation Factor Transition Analysis and Control

Based on the proof of the key role of the PFT above, two categories of PFT are defined in PFT analysis based on the pattern of PFT. PFTI is proposed as a tool to identify the dominant PFs of the concerned modes.

A. Classification of PFT

In power systems, the relationship between modes in the open-loop and closed-loop model can be divided into three types for analyzing modal interactions: two modes are in the same or different timescale, and the modes have no obvious relationship with others. The transition is analyzed based on the three types as follows.

Assume λ_p and λ_s are the open-loop eigenvalues of the wind turbine subsystem and power system subsystem concerned, and $\hat{\lambda}_p$ and $\hat{\lambda}_s$ are their corresponding closed-loop modes.

1) **Traceable Transition—PFCL**

Traceable transition refers to the transition of the PFs can be traceable from the two open-loop modes to their corresponding closed-loop modes. In other words, when the PFs of the main state variables for $\hat{\lambda}_p$ decrease compared to λ_p, the PFs of the same state variables for $\hat{\lambda}_s$ will increase the same amount compared to λ_s. It can be verified as follows.

When one open-loop mode does not affect the diagonal elements of another open-loop state space matrix, there is no change in the diagonal elements of the state space matrix, i.e., $\Delta a_{kk} = 0$. With the damping conservation character in [22], the whole power system is damping conservative.

Based on the concept in [23] and [24], for a system, no matter how the operating condition is, the sum of the real parts of all the eigenvalues of the system is a constant, equals to the sum of the diagonal elements of the state matrix, that is, the sum of the damping of all modes is constant. Therefore, the change of the variables related to the off-diagonal element F_{1i} and F_{2i} can be ignored, i.e.,

$$\sum\nolimits_{i=1}^{n}\Delta F_i = 0 \tag{12}$$

The variable ΔF_i is only related to some variables that are in the off-diagonal. When the parameters of the system are determined, ΔF_i will not have any change. In other words, the eigenvalues are always real or complex in conjugate pairs for the real matrix. Thus, the right and left eigenvectors are always complex in conjugate pairs, and so are other complex values. Therefore, the sum of the imaginary part for all similar terms is 0, which means ΔF_i can be ignored.

From (12), $\Delta\lambda_p + \Delta\lambda_s$ is irrelevant to $\Delta F_p + \Delta F_s$, and $\hat{a}_{kk}$ is an invariant constant in the closed-loop model. Therefore, $\Delta\lambda_p + \Delta\lambda_s$ is only related to the transition of PFs, i.e.,

$$real(\Delta\lambda_p + \Delta\lambda_s) = real(\sum_{k=1}^{n}\Delta p_{kp}\hat{a}_{kk(p)} + \sum_{k=1}^{n}\Delta p_{ks}\hat{a}_{kk(s)}) \tag{13}$$

For each mode in the modal interaction,

$$real(\hat{\lambda}_p) = real(\sum\nolimits_{k=1}^{n}\hat{p}_{kp}a_{kk(p)}) \tag{14}$$

$$real(\hat{\lambda}_s) = real(\sum\nolimits_{k=1}^{n}\hat{p}_{ks}a_{kk(s)}) \tag{15}$$

$$real(\lambda_p) = real(\sum\nolimits_{k=1}^{n}p_{kp}a_{kk(p)}) \tag{16}$$

$$real(\lambda_p) = real(\sum\nolimits_{k=1}^{n}p_{kp}a_{kk(p)}) \tag{17}$$

It can be concluded that the modal interactions are mainly caused by the PFT. The PFs transit just between the two modes and do not need other modes to participate in the transition to form the modal interactions. The damping conservation phenomenon in this condition means that the damping of the two concerned modes is conservative.

Definition: The phenomenon that PFs transit just between two modes and the sum of PFs of the open-loop modes is equal to the sum of PFs of the closed-loop modes is defined as participation factor conservation law (PFCL).

The mathematical expression of PFCL can be defined as follows,

$$p_{tp} = \hat{p}_{tp} + \hat{p}_{ts} \tag{18}$$

$$p_{hs} = \hat{p}_{hp} + \hat{p}_{hs} \tag{19}$$

where p_{tp} is the PF of the state variable t in the open-loop modeλ_p, and p_{hs} is the PF of the state variable h in the open-loop mode λ_s. $\hat{p}_{tp}$ and $\hat{p}_{ts}$ are the PFs of the state variable t in the closed-loop modes $\hat{\lambda}_p$and $\hat{\lambda}_s$. $\hat{p}_{hp}$ and $\hat{p}_{hs}$ are the PFs of the state variable h in the closed-loop modes $\hat{\lambda}_p$and $\hat{\lambda}_s$.

In order to determine whether the PFT in one mode is traceable, a tool named PFTI is then proposed. Using (11), we can calculate the interaction between each mode and the concerned mode and determine which modes have the most significant interaction with the concerned mode.

$$PFTI_{ki} = \frac{|PFT_{ki}|}{max|PFT_i|} \tag{20}$$

where i represents the i^{th} mode and k represents the k^{th} state variable.

If the order of the dominant state variables arranged by PFTIs is the same as that arranged by PFs, the PFT is traceable. Otherwise, it is untraceable.

2) **Untraceable Transition—BPFL**

The other category of PFT is untraceable transition, which refers to that PFT is among multiple modes, and the transition is chaotic and has no rules among these modes, resulting in obvious modal interactions.

a) Oscillation Modes in Same Timescale

The first subcategory that the modes borrow PFs are the modes in the same timescale. When the influence of one open-loop on the other open-loop is reflected in affecting the diagonal elements of the state space matrix, based on the analysis in the traceable transition, the sum of the damping for the two concerned modes is not conservational in this condition.

The above modal interactions are proposed as BPFL, which can be defined as follows: based on PFCL, the PFs are borrowed from other modes to compensate for the damping of the two concerned modes. The PFT is chaotic, making finding some rules for modal interactions hard.

$$\Delta p_{ki} \neq 0 \rightarrow \Delta\lambda_i \neq 0 \tag{21}$$

$$\Delta a_{kk} \neq 0 \rightarrow \Delta\lambda_i \neq 0 \tag{22}$$

The PFT can be described as follows,

$$real(\Delta\lambda_p + \Delta\lambda_s) = real(\sum_{k=1}^{n} PFT_{kp} + \sum_{k=1}^{n} PFT_{ks} + \sum_{k=1}^{n} PFT_{kr}) \tag{23}$$

where the subscript r represents the remaining oscillation modes apart from the two concerned modes, which means that the modal interactions cannot be formed just by the transition among the two concerned modes but by multiple modes.

Similar to PFCL, for the modes in BPFL,

$$real(\hat{\lambda}_p) = real(\sum_{k=1}^{n}(\Delta p_{kp}\hat{a}_{kk(p)} + p_{kp}\hat{a}_{kk(p)})) \tag{24}$$

$$real(\hat{\lambda}_s) = real(\sum_{k=1}^{n}(\Delta p_{ks}\hat{a}_{kk(s)} + p_{ks}\hat{a}_{kk(s)})) \tag{25}$$

$$real(\lambda_p) = real(\sum_{k=1}^{n} p_{kp}a_{kk(p)}) \tag{26}$$

$$real(\lambda_p) = real(\sum_{k=1}^{n} p_{kp}a_{kk(p)}) \tag{27}$$

It can be concluded that the damping of the two concerned modes cannot be conservative by transiting PF in just two modes. They must borrow PFs from other modes to compensate for the damping, which is a chaotic process.

Definition: The phenomenon when the concerned modes borrow PFs from other modes or the PFs of the concerned modes are borrowed by other modes is defined as borrowing participation factor law (BPFL).

b) Oscillation Modes in Different Timescale

The second subcategory that the modes borrow PFs are the modes in the different timescale. When the parameters of one open-loop mode change, the other different timescale mode will change its damping or frequency, which can be observed from the trajectories of eigenvalues. The effects may deteriorate one mode, resulting in modal resonance.

c) No Obvious Corresponding Transition Modes

Another subcategory that the modes borrow PFs to make the damping conservative is as follows. PFT corresponds to just one mode, i.e., no prominent open-loop modes are close to the concerned open-loop mode to transit PFs with it. The difference between the closed-loop and open-loop mode will be slight.

Therefore, the classification of PFT for all the modes can be presented in Fig. 2.

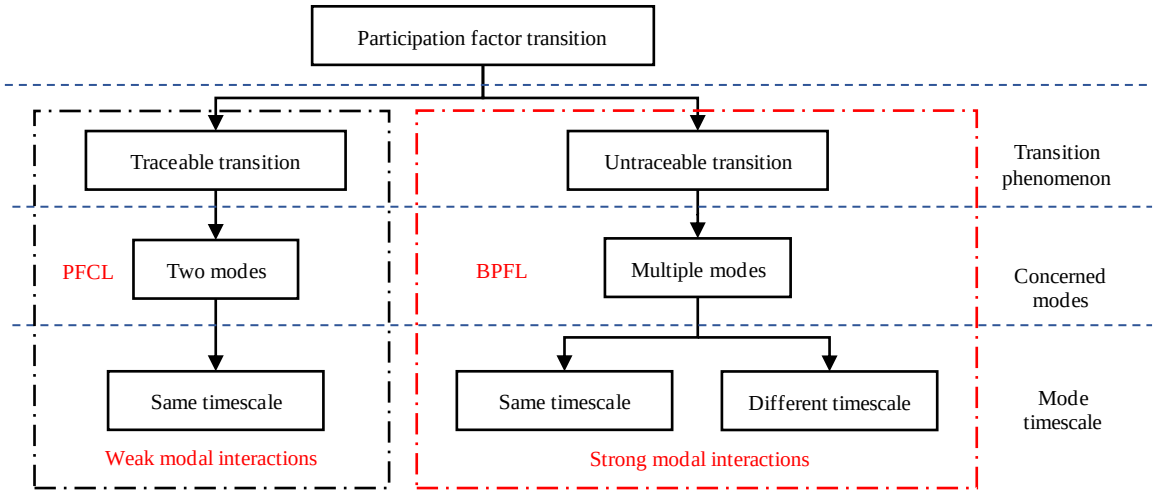

Fig. 2. Classification of participation factor transition

B. Identifying the dominant factors of PFT

Based on PFCL and BPFL, only two situations exist for two open-loop modes in the same timescale. One situation is that one mode transits enough PFs from the other to form modal interactions. PFCL reveals the situation when modal interactions can be fully covered by their own traceable PFT of the two concerned modes. These kinds of modes would not interact with the concerned mode. The other situation is that one mode cannot borrow enough PFs from the same timescale mode. It must borrow PFs from different timescale modes or those with no corresponding transition mode. Therefore, the concerned mode must borrow PFs to form the modal resonance, resulting from modal interactions in multiple modes. The state variables of the modes that belong to BPFL are selected for further analysis.

Based on BPFL, the PFT is chaotic. If the state variables ranked front by PFTIs are not the state variables ranked front by PFs, the mode would change its essence. It will result in an untraceable transition, bringing about the modal resonance in the converter-based power systems. With the proposed PFTI, the dominant associated state variables can be determined by sorting the PFTIs for multiple modes in terms of modal interactions. Previous methods, however, only infer the modal resonance phenomenon without indicating which part of the system was affected.

C. Participation factor transition control

Based on PFTI, participation factor transition control is proposed to tune the parameters that can be easily reached for the critical mode [10], decreasing the untraceable PFT and resolving the modal resonance. These parameters can be the PLL of PMSGs, PSS of synchronous generators, etc. By tuning these parameters, PFT control can make the order of state variables ranked by PFTIs the same as that ranked by PFs.

$$\begin{aligned} &Max \quad f(\lambda) = damping\ ratio\ of\ \hat{\lambda}_c \\ &s.t.\ sort\ PFTI_{di}\ according\ to\ PFs\ (d = 1, \cdots, D) \end{aligned} \tag{28}$$

where $\hat{\lambda}_c$ represents the closed-loop mode of the critical mode. D represents the number of dominant state variables of λ_i. i contains the critical mode and the mode having strong interaction with the critical mode.

The presented process uses two categories to identify the dominant state variables that cause modal resonance. It is referred to as PFT analysis. From the two categories above, it is evident that the mandatory factor for two open-loop modes to interact is the PFT. This revelation holds immense importance in enhancing the stability of converter-based power systems.

With the proposed PFT analysis and PFT control demonstrated above, the procedure of PFTAC can be given in Fig. 3.

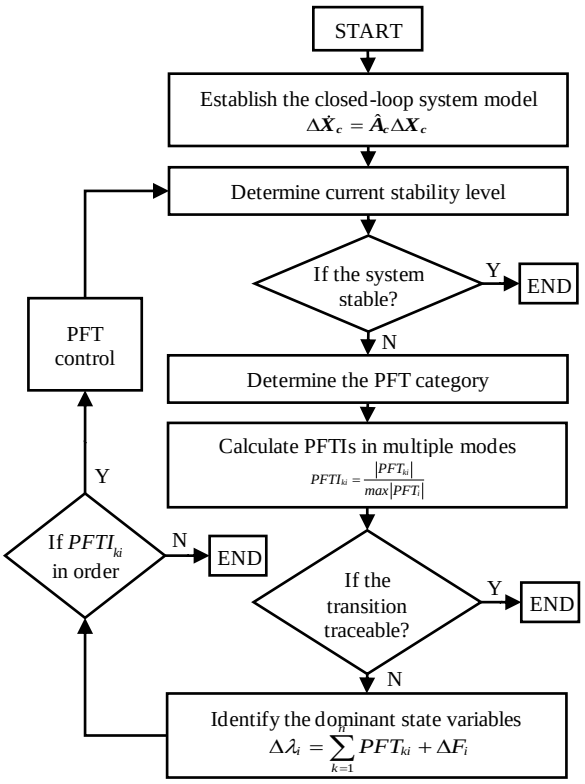

Fig. 3. Proposed participation factor transition analysis and control.

IV. Case Study

A. Example Power System

Fig. 4 shows the configuration of a converter-based two-area four-machine power system, which is used as an example power system to validate the analysis and findings made in the previous section. A 4th-order model of the SGs is used with no power system stabilizers (PSS) equipped. The loads at Bus 7 and Bus 9 are modeled as constant impedances. The detailed model and parameters of the power system are given in [25]. Two detailed 15th-order PMSGs are connected to Bus 12 and 13, respectively. PMSG adopts reactive power control with a constant power factor. G3 balances the power load flow change at slack Bus 3. Configuration and typical parameters of PMSG are listed in the Appendix.

Model PMSG2 of wind farm 2 as an open-loop wind turbine subsystem. The remaining part of the example power system is regarded as an open-loop power system subsystem, containing PMSG1. As section II shows, the open-loop state-space model of the converter-based two-area four-machine power system can be established.

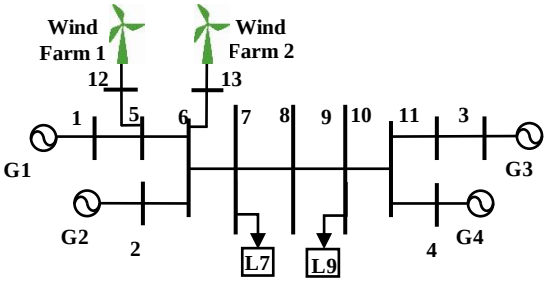

Fig. 4. Configuration of example two-area four-machine power system with PMSGs.

B. PFT analysis

There are a total of three electromechanical oscillation modes (EOMs) and four subsynchronous oscillation modes (SOMs) in the open-loop wind turbine subsystem, six EOMs and four SOMs in the open-loop power system subsystem, and nine EOMs and eight SOMs in the closed-loop system. Furthermore, there is a mode in the right plane of the coordinate system in

the closed-loop model. The proposed PFT analysis is verified in detail as follows.

1) **Traceable Transition—PFCL**

Take the *q*-axis current control inner loop of GSC as an example. λ_p is the open-loop mode of the *q*-axis current control inner loop of PMSG2 in the wind turbine subsystem, and λ_s is the open-loop mode of the *q*-axis current control inner loop of PMSG1 in the power system subsystem. These two modes are in the same timescale. $\hat{\lambda}_p$ and $\hat{\lambda}_s$ are the closed-loop modes in the closed-loop model corresponding to λ_p and λ_s. The results of PFT analysis are calculated in TABLE I.

TABLE I
RESULTS OF PFT ANALYSIS FOR TRACEABLE TRANSITION

λ_p	λ_s	$\hat{\lambda}_p$	$\hat{\lambda}_s$	$real \sum_{i=p,s} \Delta\lambda_i$	$real \sum_{i=p,s}\sum_{k=1}^{n} PFT_{ki}$
-22.9324 +98.4350*i*	-22.5030 +97.5990*i*	-22.8664 +98.3122*i*	-22.2543 +97.1371*i*	0.2464	0.2438

The calculation results fully comply with the PFCL, and the modal interactions are only related to the PFT, which verifies the definition of PFCL.

To demonstrate the PFT more clearly, the normalized PFs of the modes are shown in Fig. 5. The red bar series represents the PFs related to the *q*-axis current control inner loop of PMSG2, and the blue bar series represents the PFs related to the *q*-axis current control inner loop of PMSG1. The notations in the bar block are the main state variables of the modes. The number is the participation of these state variables. The subscripts (1) and (2) represent PMSG1 and PMSG2, respectively.

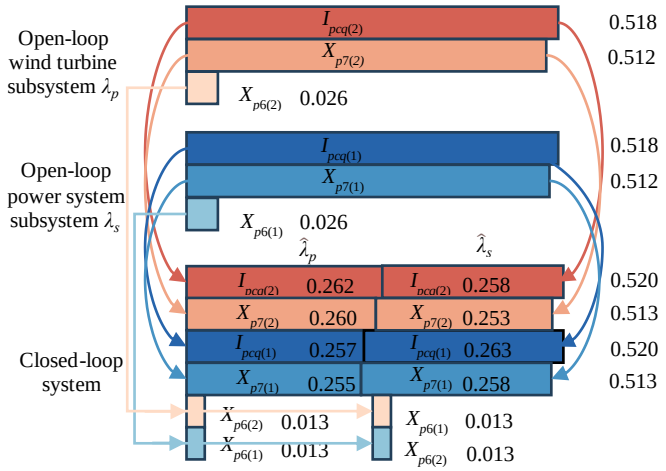

Fig. 5. Traceable transition for oscillation modes in same timescale.

According to the analysis in section II, it can be calculated that the damping of the two open-loop subsystems is -583.6108, and the damping of the closed-loop system is -583.0294. This means that this system is in accordance with the damping conservation character.

It can be seen in Fig. 5 that the state variable $I_{pcq(2)}$ consists of 0.262 in $\hat{\lambda}_p$, which decreases 0.256 compared to the participation of the corresponding open-loop mode. While in $\hat{\lambda}_s$, the participation of $I_{pcq(2)}$ increases by 0.258, which is close to its decrease in $\hat{\lambda}_p$. In other words, the increase for the participation of state variable $I_{pcq(2)}$ in $\hat{\lambda}_s$ comes from its decrease in $\hat{\lambda}_p$, which verifies the PFT. Similarly, the state variable $X_{p7(2)}$ consists of 0.260 in $\hat{\lambda}_p$, which decreases by 0.252 compared to its participation in λ_p. This number 0.252 is also close to its participation increase in $\hat{\lambda}_s$, i.e., $\lambda_p$transits PF ($X_{p7(2)}$) to λ_s to form modal interactions.

For the *q*-axis current control inner loop of the GSC in PMSG1, the participation of $I_{pcq(1)}$ in λ_s is 0.518, and the participation of $X_{p7(1)}$ is 0.512. They decrease by 0.255 and 0.254, respectively in $\hat{\lambda}_s$. These two numbers are close to their increase in $\hat{\lambda}_p$, 0.257 and 0.255. That is to say, the PFs transit traceably. The PF decrease of one mode in the closed-loop mode is the same as the increase in the other mode, and vice versa, i.e., the PF increase of one mode in the closed-loop mode comes from the PF decrease of the other mode. The orders of the PFs and the PFTIs are given in TABLE II to show the traceable PFT. The PF of the state variables for each mode in the table decreases from left to right. *rank* represents the order of state variables sorted by PFTI.

TABLE II
ORDERS OF PFS AND PFTIS FOR TRACEABLE TRANSITION

$\hat{\lambda}_p$		$I_{pcq(2)}$	$I_{pcq(1)}$	$X_{p7(2)}$	$X_{p7(1)}$	$X_{p6(2)}$	$X_{p6(1)}$
	PFTI	100%	99.98%	98.72%	98.71%	5.11%	5.08%
	rank	1	2	3	4	5	6
$\hat{\lambda}_s$		$I_{pcq(1)}$	$I_{pcq(2)}$	$X_{p7(1)}$	$X_{p7(2)}$	$X_{p6(1)}$	$X_{p6(2)}$
	PFTI	100%	99.95%	98.73%	98.68%	5.11%	5.02%
	rank	1	2	3	4	5	6

The order of the PFTIs is the same as that of the PFs, which means that the PFT can be traceable in modal interactions. The eigenvalue trajectory of the two closed-loop modes as the *q*-axis current control inner loop parameters change is shown in Fig. 6.

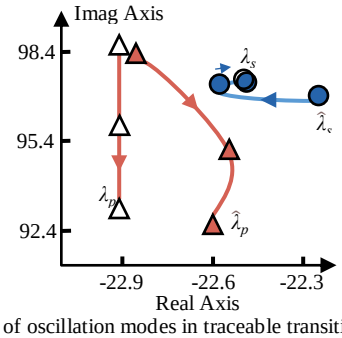

Fig. 6. Trajectories of oscillation modes in traceable transition.

The analysis above verifies (18), the defined PFCL. When the wind turbine subsystem is combined with the power system subsystem to establish the closed-loop model, the effects of the wind turbine subsystem on the power system subsystem do not act on the diagonal elements in the state space matrix corresponding to the *q*-axis current control inner loop of the GSC, i.e., $\Delta a_{kk} = 0$ (*k* represents the state variables related to *q*-axis current control inner loop of the GSC).

2) **Untraceable Transition—BPFL**

a) Oscillation Modes in Same Timescale

Take the DC voltage control outer loop of the GSC as an example. λ_p is the open-loop mode of the DC voltage control outer loop of PMSG2 in the wind turbine subsystem, and λ_s is the open-loop mode of the DC voltage control outer loop of PMSG1 in the power system subsystem. $\hat{\lambda}_p$ and $\hat{\lambda}_s$ are the closed-loop modes corresponding to λ_p and $\hat{\lambda}_s$, respectively,

in the closed-loop model. The results of PFT analysis are calculated in TABLE III. The normalized PFs of the modes in this situation are shown in Fig. 7.

TABLE III
RESULTS OF PFT ANALYSIS FOR MODES IN SAME TIMESCALE

λ_p	λ_s	$\hat{\lambda}_p$	$\hat{\lambda}_s$	real $\sum_{i=p,s}\Delta\lambda_i$	real $\sum_{i=p,s}\sum_{k=1}^{n}PFT_{ki}$
-0.0508 +0.8289i	-0.1638 +0.7524i	-0.2497 +1.3259i	0.0038 +0.7349i	-0.0313	-0.5784

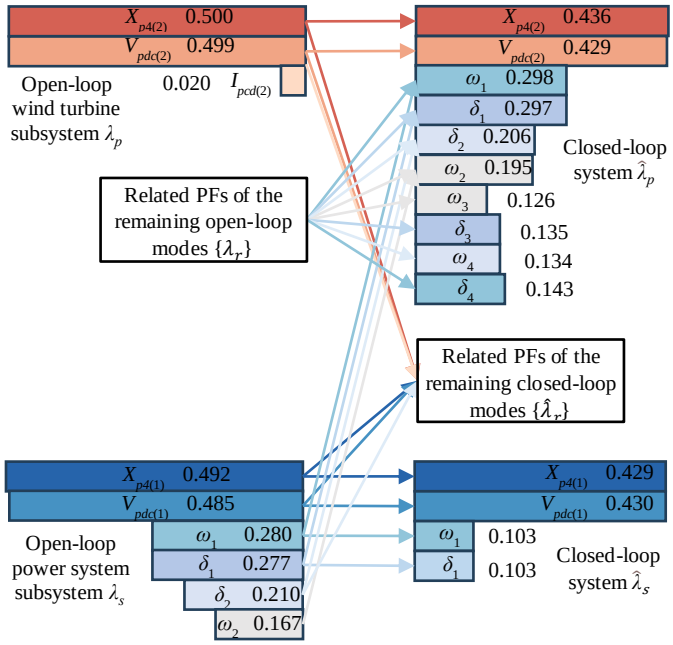

Fig. 7. Untraceable transition for oscillation modes in same timescale.

The red arrow series represents the PFT from the open-loop mode of the wind turbine subsystem to the closed-loop mode of the wind turbine subsystem or other oscillation modes apart from the two concerned modes. The blue arrow series represents the PFT from the open-loop mode of the power system subsystem to the closed-loop mode of the power system subsystem, the closed-loop mode of the wind turbine subsystem, or other oscillation modes apart from the two concerned modes. The dark arrow series represents the PFT from other open-loop oscillation modes of the power system subsystem or the wind turbine subsystem to the closed-loop mode of the power system subsystem or the wind turbine subsystem.

The two open-loop modes have large PFT to form the modal interactions, making the closed-loop modes move against each other, resulting in the modal resonance. $\hat{\lambda}_s$ will move to the right side of λ_s. When the real part of $\hat{\lambda}_p$ or $\hat{\lambda}_s$ is more significant than zero, the system will become unstable. The state variables $X_{p4(2)}$ and $V_{pdc(2)}$ consist of 0.500 and 0.499 in λ_p, which do not transit too much compared to the participation of the corresponding closed-loop mode. However, many other PFs related to the synchronous generators appear in $\hat{\lambda}_p$. Some PFs occupy more than half of the PFs in the open-loop mode. For example, the PF ω_1 in the closed-loop mode $\hat{\lambda}_p$ is 0.298, which is more than half of the participation of $X_{p4(2)}$ in λ_p. All the PFs related to the synchronous generators transit untraceable from the mode related to PMSG1 to PMSG2.

It can be seen that the damping change of these two modes cannot be only consisted of by their own PFT. These two modes must borrow damping, i.e., borrow PFs from other modes to make the damping conservative. To reveal the disorganized transition of the PFs, the orders of the PFs and the PFTIs are calculated as shown in TABLE IV

TABLE IV
ORDERS OF PFS AND PFTIS FOR MODES IN SAME TIMESCALE

		$X_{p4(2)}$	$V_{pdc(2)}$	ω_1	δ_1	ω_2	δ_2	ω_4	δ_4
$\hat{\lambda}_p$	*PFTI*	21.65%	23.71%	100%	99.44%	65.48%	69.12%	44.91%	47.91%
	rank	13	10	1	2	4	3	7	5
		$X_{p4(1)}$	$V_{pdc(1)}$	ω_1	δ_1	ω_2	δ_2	ω_4	δ_4
$\hat{\lambda}_s$	*PFTI*	30.58%	26.61%	85.30%	83.83%	79.84%	100%	42.35%	54.19%
	rank	9	10	2	3	4	1	7	5

The state variables with top ranking in PFTIs are not the state variables with top ranking in PFs, revealing the chaotic transition between the same timescale oscillation modes.

b) Oscillation Modes in Different Timescale

Take λ_p as the open-loop mode of PLL for PMSG2 in the wind turbine subsystem, which is an electromechanical mode, and λ_s as the open-loop mode of the q-axis current control inner loop of GSC for PMSG1 in the power system subsystem, which is a subsynchronous mode. $\hat{\lambda}_p$ and $\hat{\lambda}_s$ are the closed-loop modes corresponding to λ_p and λ_s, respectively, in the closed-loop model. The results of PFT analysis are calculated in TABLE V.

TABLE V
RESULTS OF PFT ANALYSIS FOR MODES IN DIFFERENT TIMESCALE

λ_p	λ_s	$\hat{\lambda}_p$	$\hat{\lambda}_s$	real $\sum_{i=p,s}\Delta\lambda_i$	real $\sum_{i=p,s}\sum_{k=1}^{n}PFT_{ki}$
-2.2831 +5.9616i	-22.5030 +97.5990i	-2.3389 +5.9876i	-22.2543 +97.1371i	0.1929	-0.0569

The eigenvalue trajectory of the two closed-loop modes as the PLL control parameters change is shown in Fig. 8. When one control parameter of the electromechanical oscillation mode changes, there will be modal interactions between the electromechanical oscillation mode and the subsynchronous oscillation mode. What is more, the interaction between these two modes will make the closed-loop electromechanical oscillation mode move to the right plane of the coordinate system, which deteriorates the stability of the system.

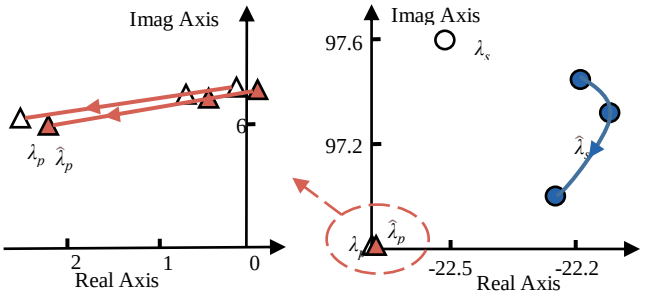

Fig. 8. Trajectories of oscillation modes in different timescale.

Based on the PFCL and the damping conservation phenomenon, in this situation, the modal interactions originate not only from their own PFT, which is not enough for consisting of their modal interactions, but also PFT from other

modes. That is to say, the PFs are borrowed from other modes to form the modal interactions, i.e., the proposed BPFL.

c) No Obvious Corresponding Transition Modes

Take the third and fourth synchronous generators as an example. λ_s is the open-loop mode of the rotor speed and angle of the fourth synchronous generator in the power system subsystem, and λ_s = -0.5162+2.0553i. $\hat{\lambda}_s$ is the closed-loop mode corresponding to λ_s, and $\hat{\lambda}_s$ = -0.5396+2.2784i. The normalized PFs of the modes are shown in Fig. 9.

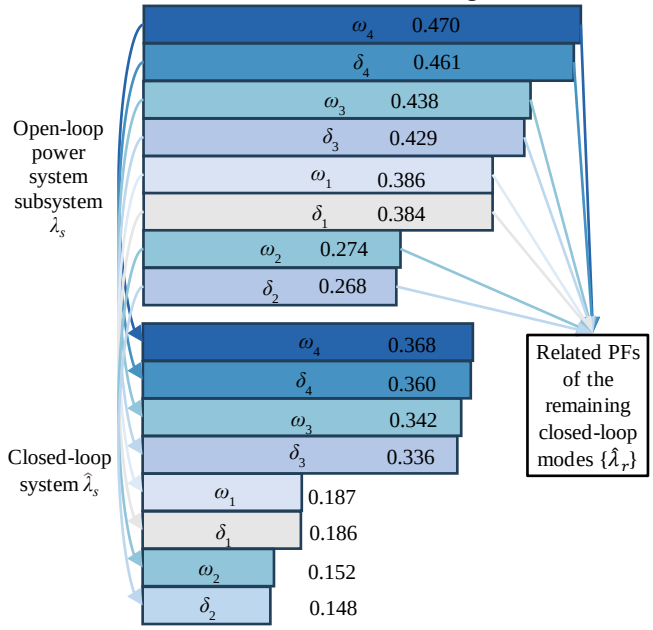

Fig. 9. PF Transition in the mode having no close modes.

There is obvious PFT between the open-loop mode and its corresponding closed-loop mode, while there are no other open-loop modes close to this mode, making the transition not that obvious to observe. PF decrease in this mode means the PFs have transited to other not close open-loop modes based on the BPFL. It can also be comprehended as other open-loop modes do not have enough PFs to form their modal interactions. Therefore, they must borrow PFs from other modes. To reveal the untraceable transition, the orders of the PFs and the PFTIs are calculated as shown in TABLE VI.

TABLE VI
ORDERS OF PFS AND PFTIS FOR MODES HAVING NO CLOSE MODES

	ω_4	δ_4	ω_3	δ_3	ω_1	δ_1	ω_2	δ_2
PFTI	0.86%	43.40%	21.38%	49.24%	30.68%	32.01%	100%	65.00%
rank	25	7	13	5	11	10	1	2

The order of the PFTIs of the dominant state variables is totally different from the order of the PFs, showing an obvious untraceable transition. The eigenvalue trajectory of the two closed-loop modes as the PLL control parameters change is shown in Fig. 10.

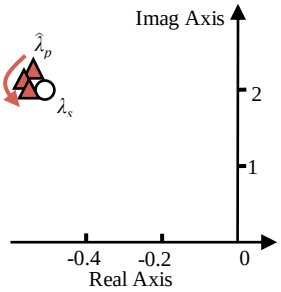

Fig. 10. PF Transition in the mode having no close modes.

3) **No Transition**

Take the q-axis current control inner loop of the MSC as an example. λ_p is the open-loop mode of the q-axis current control inner loop of PMSG2 in the wind turbine subsystem, and λ_s is the open-loop mode of the q-axis current control inner loop of PMSG1 in the power system subsystem. $\hat{\lambda}_p$ and $\hat{\lambda}_s$ are the closed-loop modes corresponding to λ_p and λ_s, respectively, in the closed-loop model. The open-loop modes and closed-loop modes are shown in TABLE VII. The normalized PFs of the modes are shown in Fig. 11.

TABLE VII
Q-AXIS CURRENT CONTROL INNER LOOP MODES OF MSC

λ_p	λ_s	$\hat{\lambda}_p$	$\hat{\lambda}_s$
-2.1846+22.2055i	-2.1846+22.2055i	-2.1846+22.2055i	-2.1846+22.2055i

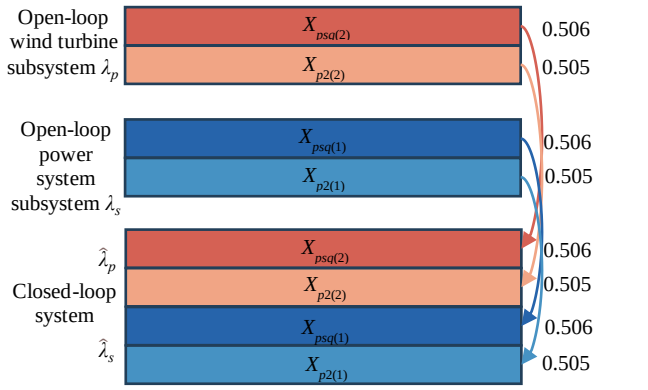

Fig. 11. No transition in PFs.

No PFs transit in the two modes, and it can be calculated that $\Delta p_{ki} = 0$, $\Delta a_{kk} = 0$, which is consistent with PFCL. These kinds of modes do not need to be considered in modal interactions.

C. PFT control

The critical mode belongs to the power system subsystem. The modes in Table VIII belong to BPFL and may have a significant interaction with the critical mode. PFT in the table represents the interaction amount of the corresponding mode in the critical mode.

TABLE VIII
MODES BELONG TO BPFL IN THE TWO-AREA FOUR-MACHINE POWER SYSTEM

Mode	λ	$\hat{\lambda}$	State variable	PFT
1	-2.2831+5.9616i	-2.3389+5.9876i	$X_{pll(2)}$ $\theta_{pll(2)}$	2.2825 + 0.8742i
2	-2.2510+5.9250i	-2.2362+5.9396i	$X_{pll(1)}$ $\theta_{pll(1)}$	-0.0099 + 0.0085i
3	-0.5162+2.0553i	-0.5396+2.2784i	ω_4 θ_4	-0.1156 - 0.0744i
4	0.4146+3.4768i	0.4668+3.5182i	ω_2 θ_2	-0.0885 + 0.1020i
5	-97.6811+0.2765i	-97.7130+0.2203i	E_{fd2} E_{fd1}	-0.0885 + 0.1020i

From the above table, Mode 1 is the main reason for the modal resonance. The real part of the modal interactions is positive, resulting in the mode of the power system subsystem moving to the right plane of the coordinate system. The orders of the PFs and the PFTIs of Mode 1 are calculated as shown in TABLE IX.

TABLE IX
ORDERS OF PFS AND PFTIS FOR MODE 1

	$\theta_{pll(2)}$	$X_{pll(2)}$	ω_2	δ_2	$X_{p6(2)}$	E_{q2}	E_{q1}	ω_1
PFTI	38.31%	39.76%	100%	96.34%	43.62%	19.01%	10.21%	10.13%
rank	5	4	1	2	3	6	7	8

The PFTIs are ordered differently from the order of PFs. Apply the moth-flame optimization algorithm (MFO) in PFT control to tune the parameters of PLL. The critical mode 0.0038 +0.7349*i* will change to stable mode -0.0465 + 0.7873*i*. The trajectory of these two modes in this situation is displayed in Fig. 12.

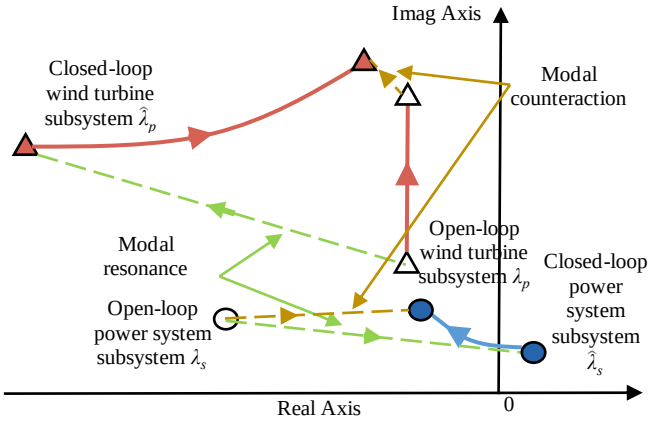

Fig. 12. Trajectory of the modes in PFT control

In Fig. 12, the green lines represent the modal resonance, and the brown lines represent the modal counteraction. PFT control is used to optimize modal resonance to modal counteraction. The arrow directions on the green and brown lines represent the change from the open-loop modes to the closed-loop modes. The red and blue lines represent the change of different modes. For example, the blue line represents the change of the closed-loop power system subsystem mode, and the arrow direction represents the trajectory from modal resonance to modal counteraction, revealing the process of PFT control. Once the interaction of these two modes changes from modal resonance to modal counteraction, the system becomes stable [26]. The PFTIs in Table X in this condition show that the PFT of the dominant state variables is much less than the condition of the modal resonance. And the state variables that have the largest PFTIs would change to the ones that dominate the modes. PFTIs of the state variables are ordered the same as the PFs and there is no modal resonance in this condition, which indicates that the modal resonance is mainly caused by the untraceable PFT. It verifies the proposed PFT control to be useful for improving the small-signal stability of the converter-based power systems.

TABLE X
ORDERS OF PFS AND PFTIS FOR MODES IN MODAL COUNTERACTION

$\hat{\lambda}_s$		$X_{p4(2)}$	$V_{pdc(2)}$	$X_{p4(1)}$	$V_{pdc(1)}$	ω_1	δ_1	ω_2	δ_2
	PFTI	100%	98.52%	84.09%	82.90%	69.67%	68.77%	38.27%	28.75%
	rank	1	2	3	4	5	6	7	8
$\hat{\lambda}_p$		$X_{p4(1)}$	$V_{pdc(1)}$	$X_{p4(2)}$	$V_{pdc(2)}$	ω_1	δ_1	ω_2	δ_2
	PFTI	100%	99.93%	77.75%	77.50%	8.25%	8.24%	4.18%	4.01%
	rank	1	2	3	4	5	6	7	8
$\hat{\lambda}_4$		$\theta_{pll(2)}$	$X_{pll(2)}$	$\theta_{pll(1)}$	$X_{pll(1)}$	ω_2	δ_2	$X_{p6(2)}$	ω_1
	PFTI	100%	99.78%	94.11%	93.75%	10.36%	9.99%	4.11%	4.10%
	rank	1	2	3	4	5	6	7	8

D. Validation in a Converter-based New England Power System

Fig. 13 presents the configuration of a converter-based New England power system. The simplified 3rd-order model of the SGs and a 1st-order of the automatic voltage regulator (AVR) are adopted. The parameters of the example system are given in [27].

The following results can be obtained based on the proposed participation factor transition analysis and control.

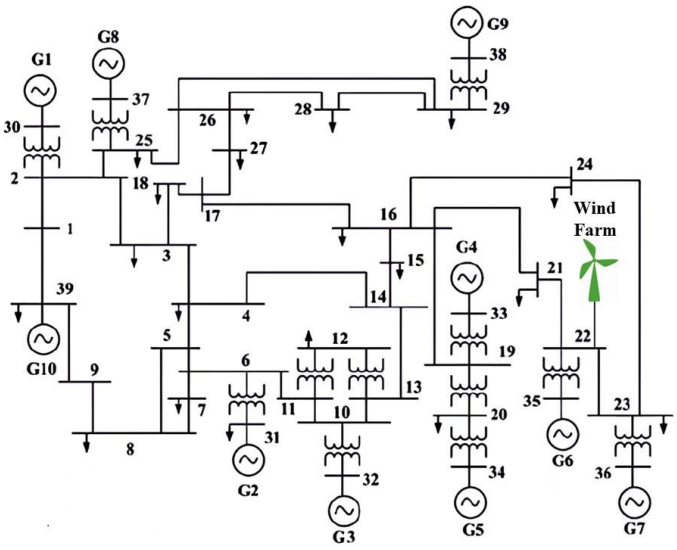

Fig. 13. Configuration of the converter-based New England power system.

1) **Network Modelling**

Model the wind farm as an open-loop wind turbine subsystem and the remaining part of the example power system as an open-loop power system subsystem.

2) **Determine Stability**

In the closed-loop system, one mode related to the power system subsystem is in the right plane of the coordinate system, which influences the small-signal stability.

3) **Determine the PFT category**

Ignore the modes that belong to the categories "Traceable Transition-PFCL" and "No transition", for example, the electromechanical mode related to the 8th SG and the mode related to the d-axis current control inner loop of MSC in PMSG. The normalized PFs of the mode related to the 8th SG are shown in Fig. 14.

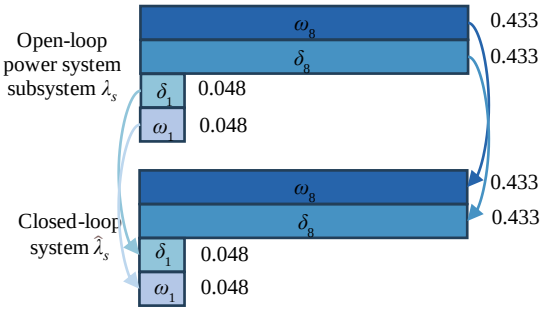

Fig. 14. No transition category in New England power system.

4) **Calculate PFT in multiple modes**

The mode $\hat{\lambda}_{s1}$=0.0487+ 2.8855*i*, influencing the small-signal stability, is related to the rotor angle and the angular speed of the 10th SG. The modal interactions among multiple modes are shown in Fig. 15.

Table XI shows the modes belonging to BPFL and may have significant interaction with the critical mode.

TABLE XI
MODES BELONG TO BPFL IN NEW ENGLAND POWER SYSTEM

Mode	λ	$\hat{\lambda}$	State variable	PFT
1	-0.1218+3.2304*i*	-0.2502+3.3472*i*	X_{pll} θ_{pll}	0.2409 - 6.4201i
2	-0.3332+0.3147*i*	-0.4229+0.0216*i*	State variables related to SGs	0.0017 - 0.0026*i*

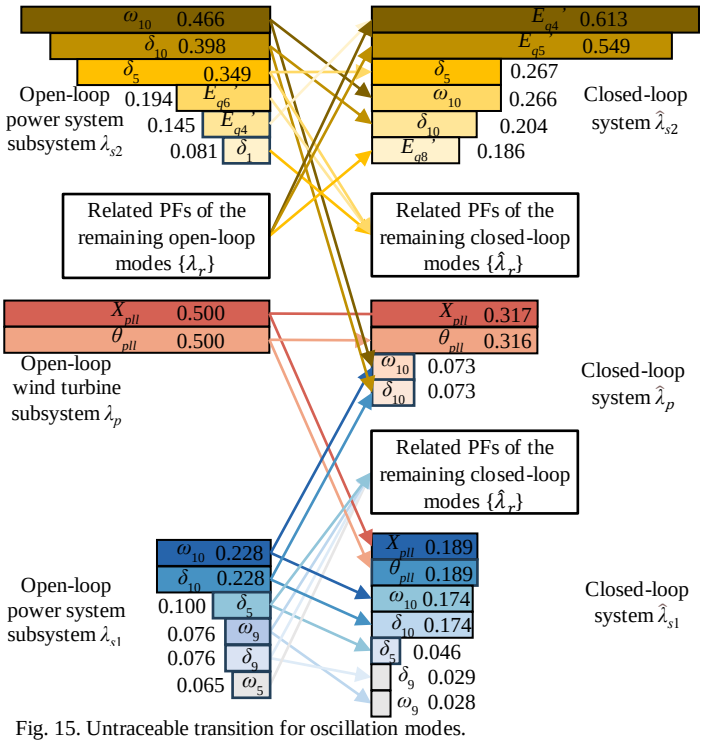

Fig. 15. Untraceable transition for oscillation modes.

5) **Identifying the dominant factors of PFT**

From the above table, the mode related to PLL and the mode related to the state variables of SGs are the main reason for the modal resonance. The real part of the modal interactions is positive, resulting in the mode of the power system subsystem moving to the right plane of the coordinate system.

Calculate the PFTIs in Table XII.

TABLE XII
ORDERS OF PFS AND PFTIS IN MODAL RESONANCE

		X_{pll}	θ_{pll}	ω_{10}	δ_{10}	δ_5	ω_9
$\hat{\lambda}_p$	*PFTI*	100%	99.91%	52.85%	52.91%	15.60%	6.79%
	rank	1	2	3	4	5	10
		E_{q4}	E_{q5}	δ_5	ω_{10}	δ_{10}	E_{q8}'
$\hat{\lambda}_{s2}$	*PFTI*	95.96%	100%	16.83%	40.82%	39.82%	1.16%
	rank	2	1	7	3	4	32

6) **PFT control**

Based on the PFTIs above, the parameters of the 4th SG and PLL are the main reasons for the modal resonance. In this paper, the parameters of PLL are optimized in PFT control. The critical mode will change to stable mode -0.2308 + 3.1722*i* by applying MFO in PFT control to tune the parameters of PLL. The trajectory of these modes in this situation is displayed in Fig. 16. Table XIII shows the PFTIs in the condition of the modal counteraction. And the state variables that have the largest PFTIs would change to the ones that dominate the modes. PFTIs of the state variables would be ordered the same as the PFs. Then the proposed PFTAC is verified to be highly useful for improving the small-signal stability of the converter-based power systems.

TABLE XIII
ORDERS OF PFS AND PFTIS FOR MODE 2 IN MODAL COUNTERACTION

		X_{pll}	θ_{pll}	ω_{10}	δ_{10}	δ_5	ω_9
$\hat{\lambda}_p$	*PFTI*	100%	99.52%	53.07%	52.98%	19.76%	17.84%
	rank	1	2	3	4	5	6
		E_{q5}	E_{q3}	δ_5	ω_{10}	δ_{10}	E_{q6}
$\hat{\lambda}_{s2}$	*PFTI*	100%	35.67%	26.83%	15.58%	15.04%	3.89%
	rank	1	2	3	4	5	8

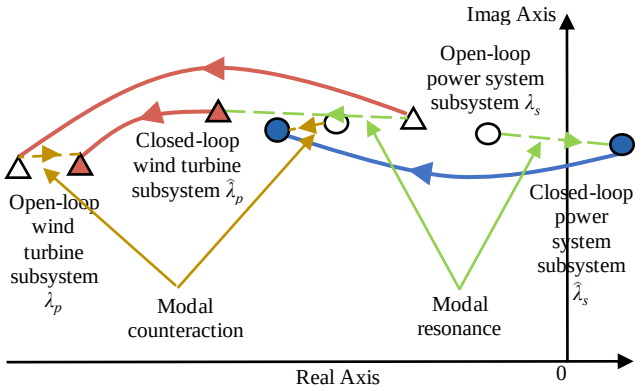

Fig. 16. Trajectory of the modes in PFT control.

To further validate the effectiveness of PFT control, time-domain simulations are also carried out. Near strong/weak modal resonance and the optimized modal interaction obtained by PFT control are compared. The disturbance is set to be at t=0.2s; a three-phase-to-earth short circuit occurs at Bus 1 and subsequently clears after 100ms. The performance of multiple modes is shown in Fig. 17. Compared with the near strong/weak modal resonance, with the proposed PFT, it is noteworthy that the critical mode is improved while other modes belonging to BPFL also have an acceptable damping ratio. Once the near strong modal resonance condition happens, PFT control can be implemented to eliminate the resonance.

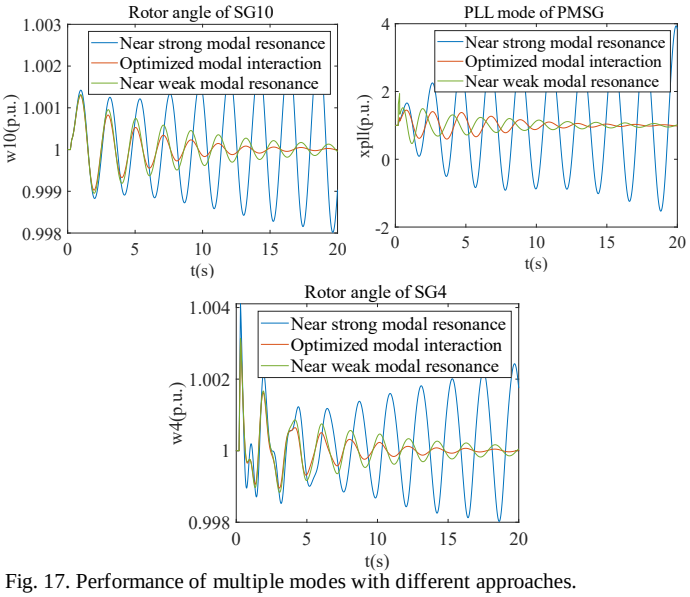

Fig. 17. Performance of multiple modes with different approaches.

The bus voltage and active power output at PCC of PMSG and SG10 are illustrated in Fig. 18. If PFT is not properly controlled, near strong resonance may deteriorate the damping of the system. With the proposed PFT control, the strong/weak resonance will be eliminated. The time-domain responses of PMSG and SGs indicate that the performance of the closed-loop power system is improved.

E. Validation in a Converter-based Practical Power System

Fig. 19 presents the configuration of a converter-based practical power system [28]. A wind farm is integrated into the system through bus 14. The simplified 3rd-order model of the SGs and a 1st-order of the automatic voltage regulator (AVR) are adopted.

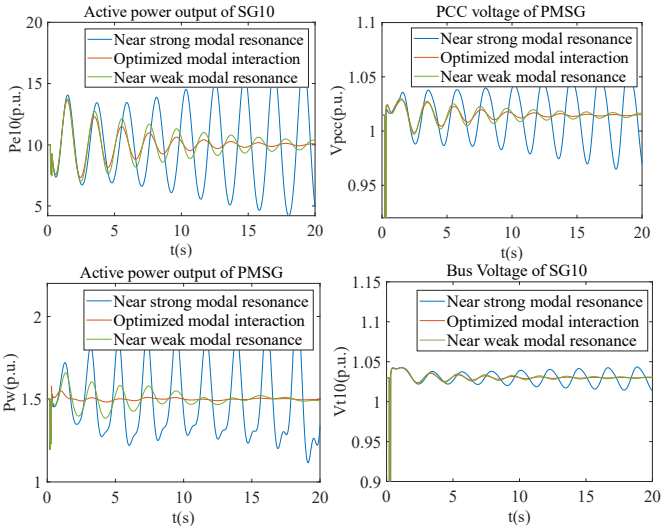

Fig. 18. Performance comparison of PMSG and SG10 with different approaches.

The following results can be obtained based on the proposed participation factor transition analysis and control.

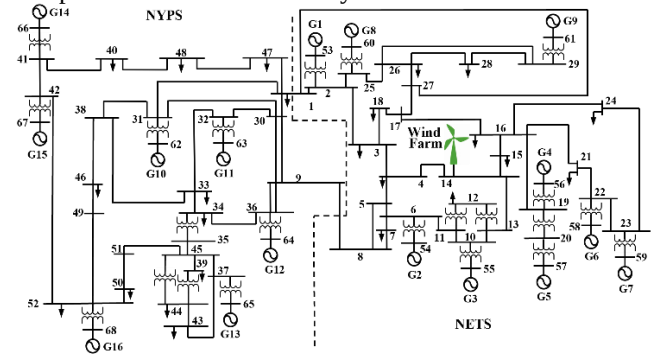

Fig. 19. Configuration of the converter-based practical power system.

1) **Network Modelling**

Model the wind farm as an open-loop wind turbine subsystem and the remaining part of the example power system as an open-loop power system subsystem.

2) **Determine Stability**

In the closed-loop system, one mode related to the power system subsystem is in the right plane of the coordinate system, which influences the small-signal stability.

3) **Determine the PFT category**

Ignore the modes that belong to the categories "Traceable Transition-PFCL" and "No transition".

4) **Calculate PFT in multiple modes**

The critical mode $\hat{\lambda}_p = 0.0902 + 2.8666i$, influencing the small-signal stability, is related to the PLL of PMSG. The modal interactions among multiple modes are similar to Fig. 13.

Table XIV shows the modes belonging to BPFL and may have significant interaction with the critical mode.

TABLE XIV
MODES BELONG TO BPFL IN NEW ENGLAND POWER SYSTEM

Mode	λ	$\hat{\lambda}$	State variable	PFT
1	-0.2578+3.7612i	-0.4869+3.6367i	State variables related to SGs	0.1883+0.0562i
2	-0.0868+4.1314i	-0.0878+4.1360i	State variables related to SGs	0.1577-0.0015i
3	-0.0536+5.3870i	-0.0539+5.3859i	State variables related to SGs	0.1437-0.0157i

5) **Identifying the dominant factors of PFT**

From the above table, the mode related to PLL and the mode related to the state variables of SGs are the main reasons for the modal resonance.

Calculate the PFTIs in Table XV.

TABLE XV
ORDERS OF PFS AND PFTIS IN MODAL RESONANCE

$\hat{\lambda}_{s1}$		X_{pll}	θ_{pll}	x_{p6}	ω_9	δ_9	ω_{13}	δ_{13}
	PFTI	100%	99.23%	38.81%	11.81%	11.81%	24.93%	24.93%
	rank	1	2	3	7	6	5	4
$\hat{\lambda}_{s2}$		δ_{16}	ω_{16}	ω_{14}	δ_{14}	ω_{15}	δ_{15}	ω_{13}
	PFTI	7.75%	7.75%	100%	100%	39.71%	39.71%	17.62%
	rank	29	28	1	2	7	8	23
$\hat{\lambda}_{s3}$		δ_{15}	ω_{15}	ω_{14}	δ_{14}	ω_{16}	δ_{16}	E_{q14}
	PFTI	100%	100%	9.62%	9.62%	18.46%	18.46%	0.29%
	rank	1	2	19	18	8	7	46

Based on the PFTIs above, the parameters of the 15th SG and PLL are the main reasons for the modal resonance. In this paper, the parameters of PLL are optimized in PFT control. The critical mode will change to stable mode -0.2340 + 2.5067i by applying MFO in PFT control to tune the parameters of PLL. The trajectory of these modes in this situation is displayed in Fig. 20.

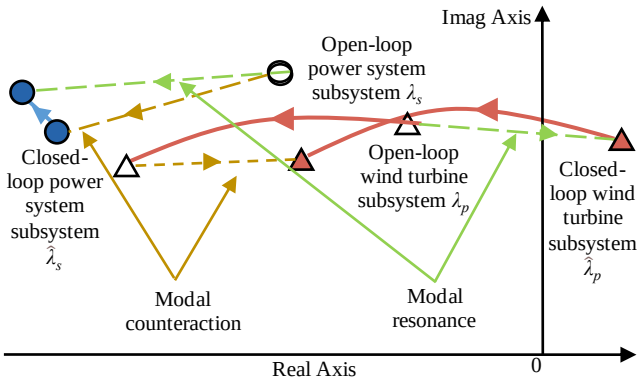

Fig. 20. Trajectory of the modes.

Table XVI shows the PFTIs in the condition of the modal counteraction. And the state variables that have the largest PFTIs would change to the ones that dominate the modes. PFTIs of the state variables would be ordered the same as the PFs.

TABLE XVI
ORDERS OF PFS AND PFTIS IN MODAL RESONANCE

$\hat{\lambda}_{s1}$		X_{pll}	θ_{pll}	x_{p6}	ω_9	δ_9	ω_{15}	δ_{15}
	PFTI	100%	97.20%	71.26%	40.82%	40.82%	18.21%	18.21%
	rank	1	2	3	4	5	6	7
$\hat{\lambda}_{s2}$		δ_{16}	ω_{16}	ω_{14}	δ_{14}	ω_{15}	δ_{15}	ω_{13}
	PFTI	100%	100%	66.16%	66.16%	52.32%	52.31%	47.35%
	rank	1	2	3	4	5	6	7
$\hat{\lambda}_{s3}$		δ_{15}	ω_{15}	ω_{14}	δ_{14}	ω_{16}	δ_{16}	E_{q14}
	PFTI	100%	100%	37.66%	37.66%	23.35%	23.35%	0.26%
	rank	1	2	3	4	5	6	48

To further validate the effectiveness of PFT control, time-domain simulations are also carried out. Near strong/weak modal resonance and the optimized modal interaction obtained by PFT control are compared. The disturbance is set to be at t=0.2s; a three-phase-to-earth short circuit occurs at Bus 1 and subsequently clears after 20ms. The performance of multiple modes is shown in Fig. 21. Compared with the near strong/weak modal resonance, with the proposed PFT, the

critical mode is improved while other modes belonging to BPFL also have an acceptable damping ratio.

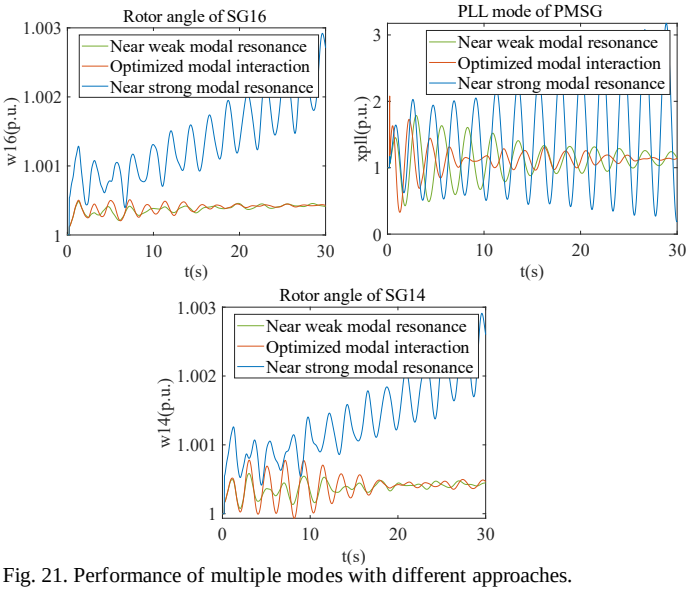

Fig. 21. Performance of multiple modes with different approaches.

The bus voltage and active power output at PCC of PMSG and SG16 are illustrated in Fig. 22. With the proposed PFT control, the strong/weak resonance is eliminated. The time-domain responses indicate that the performance of the closed-loop power system is improved. Then the proposed PFTAC is verified to be highly useful for improving the small-signal stability of the converter-based power systems.

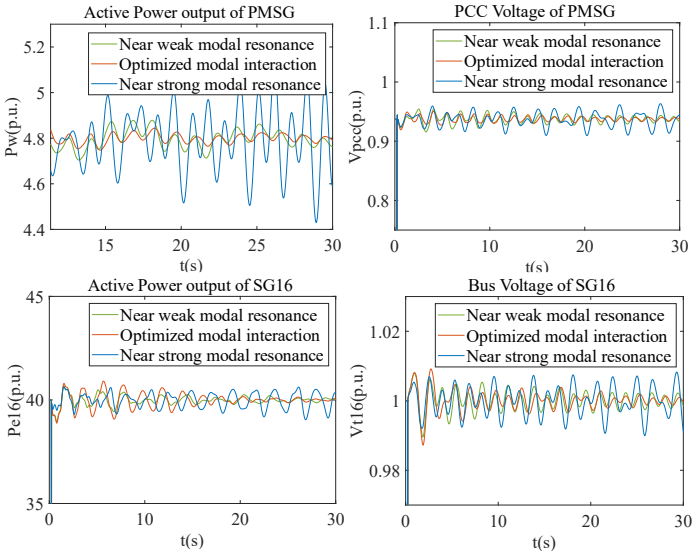

Fig. 22. Performance comparison of PMSG and SG16 with different approaches.

V. Conclusion

The extensive utilization of renewable energy resources in power systems has brought different timescale oscillation issues. This paper proposes a PFTAC method to solve the oscillation issues of the converter-based power system. The main conclusions are summarized as follows.

This paper proposes PFT to quantitatively prove the interaction among open-loop modes is caused by PFT, which is also the essential mechanism of modal resonance. Two distinct categories of PFT phenomena are further defined in PFT analysis to illustrate the relationship between modal interactions and PFT, unfolding the criticality of PFT among multiple modes in modal interactions for the first time.

PFTI is proposed to select the untraceable modes and then identify the associated state variables of modal interactions. PFT control is further proposed to solve the modal resonance based on the results of PFT analysis and PFTI. The effectiveness of PFTAC is successfully demonstrated through validation in the converter-based power systems, verifying that the modal resonance is caused by the state variables with dominant PFT among multiple modes rather than the dominant PFs of the two concerned modes. These findings contribute value to our understanding of PFs in converter-based power system dynamics and offer insights into mitigating small-signal stability issues associated with renewable energy sources.

Appendix

A. Two-open-loop Linearized Model of the Converter-based Power System

The wind turbine subsystem refers to a direct-drive wind turbine. Select the small-signal increment of the wind turbine output current $\Delta \boldsymbol{I}$ and terminal voltage $\Delta \boldsymbol{V}$ as the interface variable between the wind turbine and the power system subsystem. Let $\boldsymbol{X_p}$ be the column vector composed of all state variables of the wind turbine. The open-loop state-space model of the wind turbine subsystem can be obtained,

$$\begin{cases} \Delta \dot{\boldsymbol{X}}_p = \boldsymbol{A_p} \Delta \boldsymbol{X}_p + \boldsymbol{B_p} \Delta \boldsymbol{V} \\ \Delta \boldsymbol{I} = \boldsymbol{C_p} \Delta \boldsymbol{X}_p + \boldsymbol{D_p} \Delta \boldsymbol{V} \end{cases} \tag{A1}$$

where $\boldsymbol{A_p}$ is the corresponding state space matrix of the wind turbine subsystem. $\boldsymbol{B_p}$, $\boldsymbol{C_p}$ and $\boldsymbol{D_p}$ are the corresponding coefficient matrices of the wind turbine subsystem.

In terms of PMSG, $\boldsymbol{X_p} = [\psi_{psd}\ \psi_{psq}\ \omega_{pr}\ x_{p1}\ x_{p2}\ x_{p3}\ \Delta I_{pcd}\ \Delta I_{pcq}\ \Delta V_{pdc}\ x_{p4}\ x_{p5}\ x_{p6}\ x_{p7}\ x_{pll}\ \theta_{pll}]^T$. ψ_{psd} and ψ_{psq} are the direct and quadrature axis flux linkage of the stator winding. ω_{pr} is the angular speed of generator mass. x_{p1}, x_{p2} and x_{p3} are state variables in different control loops of MSC. I_{pcd} and I_{pcq} are the *d* and *q-axis* components of output current from the GSC, respectively. V_{pdc} is the DC voltage across the capacitor. x_{p4}, x_{p5}, x_{p6} and x_{p7} are state variables in different control loops of GSC. x_{pll} is the state variable related to the control loop of PLL. θ_{pll} is the tracked phase, which is taken as the direction of the *d*-axis of the *d-q* coordinates of the GSC. $\Delta \boldsymbol{V} = [\Delta V_x, \Delta V_y]$ is the voltage variation of PCC, and $\Delta \boldsymbol{I}=[\Delta I_x, \Delta I_y]^T$ is the current injection variation from PMSG at PCC under the standard x-y coordinate system.

Let $\boldsymbol{X_s}$ be the column vector composed of all state variables of the power system subsystem. The open-loop state-space model of the power system subsystem can be obtained,

$$\begin{cases} \Delta \dot{\boldsymbol{X}}_s = \boldsymbol{A_s} \Delta \boldsymbol{X}_s + \boldsymbol{B_s} \Delta \boldsymbol{I} \\ \Delta \boldsymbol{V} = \boldsymbol{C_s} \Delta \boldsymbol{X}_s + \boldsymbol{D_s} \Delta \boldsymbol{I} \end{cases} \tag{A2}$$

where $\boldsymbol{A_s}$ is the corresponding state space matrix of the power system subsystem. $\boldsymbol{B_s}$, $\boldsymbol{C_s}$ and $\boldsymbol{D_s}$ are the corresponding coefficient matrices of the power system subsystem.

For the case study, $\boldsymbol{X_s} = [\boldsymbol{X_G}, \boldsymbol{X_{p1}}]^T$, $\boldsymbol{X_G} = [\boldsymbol{X_{G1}}, \boldsymbol{X_{G2}}, \boldsymbol{X_{G3}}, \boldsymbol{X_{G4}}]^T$, $\boldsymbol{X_{Gi}}$, i = 1, 2, 3, 4 denotes the vector of all the state

variables of the i^{th} SG. $\boldsymbol{X_G} = [\delta\ \omega\ E_q'\ E_{fd}]^T$. δ is the rotor angle of the SG. ω is the angular speed of the SG. E_q' is the q-axis transient electromotive force. E_{fd} is the output voltage of AVR. $\boldsymbol{X_{p1}}$ is the vector of all the state variables of the other PMSG, and the state variables are the same as the wind turbine subsystem.

B. The Control Strategy of the Converter for PMSG

The machine-side converter of PMSG adopts vector control, and its control strategy is shown in Fig. A1.

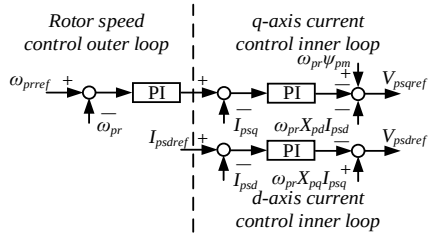

Fig. A1. Configuration of the control system of the MSC of the PMSG

where K_{pi1}, K_{pi2} and K_{pi3} are the gains of integral controllers, and K_{pp1}, K_{pp2} and K_{pp3} are the gains of the proportional controller. X_{pd} and X_{pq} are the d and q axis reactance for stator windings, respectively. I_{psd} and I_{psq} are the current of PMSG, I_{psdref} and I_{psqref} are their relevant references, and V_{psdref} and V_{psqref} are corresponding terminal voltage references. ω_{pr} is the angular speed of PMSG, and ω_{prref} is the reference of ω_{pr}. ψ_{pm} is the flux of the permanent magnet.

The control strategy of the grid-side converter is shown in Fig. A2.

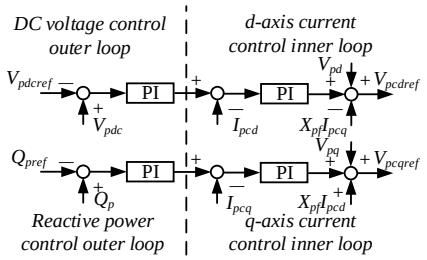

Fig. A2. Configuration of the control system of the GSC of the PMSG

where I_{pcd} and I_{pcq} are the d and q-axis components of output current from the GSC, respectively; V_{pcd} and V_{pcq} are the references of terminal voltage; V_{pd} and V_{pq} are the voltage of the PCC; V_{pdc} is the DC voltage across the capacitor; Q_{pref} is the reference of reactive power control outer loop; I_{pcdref} and I_{pcqref} are the references of current control inner loops; V_{pdcref} is the reference of DC voltage control outer loop; Q_p is the reactive power output from the GSC

C. Parameters of the Case Study

Parameters of the modified converter-based two-area four-machine power system are shown in the tables below.

TABLE AI
BASIC PARAMETERS OF PMSG (p.u.)

R_{ps}	X_{pd}	X_{pq}	X_{pf}	C_p	ψ_{pm}
0	0.2	0.2	0.02	30	1

TABLE AII
PI GAINS OF MSC, GSC, AND PLL CONTROLLERS FOR PMSG

K_{pp1}	K_{pp2}	K_{pp3}	K_{pp4}	K_{pp5}	K_{pp6}	K_{pp7}	K_{pll}
5	2	1	2	0.5	1	0.5	4.4

K_{pi1}	K_{pi2}	K_{pi3}	K_{pi4}	K_{pi5}	K_{pi6}	K_{pi7}	K_{pill}
20	200	100	20	100	10	100	39.27

REFERENCES

[1] G. J. Schaeffer and P. Vaessen, "Future power system transition - step into the light," 2005 International Conference on Future Power Systems, Amsterdam, Netherlands, 2005, pp. 6 pp.-6, doi: 10.1109/FPS.2005.204257.

[2] S. M. Ashabani and Y. A. -r. I. Mohamed, "New Family of Microgrid Control and Management Strategies in Smart Distribution Grids—Analysis, Comparison and Testing," in IEEE Transactions on Power Systems, vol. 29, no. 5, pp. 2257-2269, Sept. 2014, doi: 10.1109/TPWRS.2014.2306016.

[3] C. Wu, Y. Lyu, Y. Wang and F. Blaabjerg, "Transient Synchronization Stability Analysis of Grid-following Converter Considering the Coupling Effect of Current Loop and Phase Locked Loop," in IEEE Transactions on Energy Conversion, doi: 10.1109/TEC.2023.3314095.

[4] N. Verma, N. Kumar and R. Kumar, "Battery energy storage-based system damping controller for alleviating sub-synchronous oscillations in a DFIG-based wind power plant," in Protection and Control of Modern Power Systems, vol. 8, no. 2, pp. 1-18, April 2023, doi: 10.1186/s41601-023-00309-7.

[5] S. Singh, S. Saini, S. K. Gupta and R. Kumar, "Solar-PV Inverter for the Overall Stability of Power Systems with Intelligent MPPT Control of DC-Link Capacitor Voltage," in Protection and Control of Modern Power Systems, vol. 8, no. 1, pp. 1-20, January 2023, doi: 10.1186/s41601-023-00285-y.

[6] W. Du, J. Bi and H. Wang, "Damping Degradation of Power System Low-Frequency Electromechanical Oscillations Caused by Open-Loop Modal Resonance," in IEEE Transactions on Power Systems, vol. 33, no. 5, pp. 5072-5081, Sept. 2018, doi: 10.1109/TPWRS.2018.2805187.

[7] W. Du, X. Chen and H. F. Wang, "Power System Electromechanical Oscillation Modes as Affected by Dynamic Interactions From Grid-Connected PMSGs for Wind Power Generation," in IEEE Transactions on Sustainable Energy, vol. 8, no. 3, pp. 1301-1312, July 2017, doi: 10.1109/TSTE.2017.2677094.

[8] W. Du, Y. Wang, H. Wang and Q. Fu, "Concept of Modal Repulsion for Examining the Sub-Synchronous Oscillations in Power Systems," in IEEE Transactions on Power Systems, vol. 33, no. 4, pp. 4614-4624, July 2018, doi: 10.1109/TPWRS.2018.2790171.

[9] W. Du, Q. Fu, H. Wang and Y. Wang, "Concept of Modal Repulsion for Examining the Subsynchronous Oscillations Caused by Wind Farms in Power Systems," in IEEE Transactions on Power Systems, vol. 34, no. 1, pp. 518-526, Jan. 2019, doi: 10.1109/TPWRS.2018.2862883.

[10] J. Luo, S. Bu, J. Zhu and C. Y. Chung, "Modal Shift Evaluation and Optimization for Resonance Mechanism Investigation and Mitigation of Power Systems Integrated With FCWG," in IEEE Transactions on Power Systems, vol. 35, no. 5, pp. 4046-4055, Sept. 2020, doi: 10.1109/TPWRS.2020.2975631.

[11] Q. Chen and S. Bu, "Impedance-Based Stability Analysis of Power System Wideband Oscillations: A Bridge between s Domain and Frequency Domain," in IEEE Transactions on Power Systems, 2023, (Early access) doi: 10.1109/TPWRS.2023.3341432.

[12] Q. Chen, S. Bu and C. Y. Chung, "Small-Signal Stability Criteria in Power Electronics-Dominated Power Systems: A Comparative Review," in Journal of Modern Power Systems and Clean Energy, 2023, (Early access) doi: 10.35833/MPCE.2023.000526.

[13] B. Shao, Q. Xiao, L. Wang, P. Han, Z. Bin, C. Wang, F. Blaabjerg and Z. Chen, "Review on power system generalized modal resonance analysis", International Journal of Electrical Power & Energy Systems, 154, (2023), 109417. DOI: 10.1016/j.ijepes.2023.109417.

[14] Y. Hu, S. Zhao and Y. Ma, "Study on failure of PSS caused by instability of close mode shapes," 2011 4th International Conference on Electric Utility Deregulation and Restructuring and Power Technologies (DRPT), Weihai, China, 2011, pp. 1747-1750, doi: 10.1109/DRPT.2011.5994180.

[15] B. Shao et al., "Participation Factors Instability and Analysis of Direct-Drive Wind Farms with VSC-HVDC Systems," 2022 IEEE Power & Energy Society General Meeting (PESGM), Denver, CO, USA, 2022, pp. 01-05, doi: 10.1109/PESGM48719.2022.9917016.

[16] W. A. Hashlamoun, M. A. Hassouneh and E. H. Abed, "New Results on Modal Participation Factors: Revealing a Previously Unknown Dichotomy," in IEEE Transactions on Automatic Control, vol. 54, no. 7, pp. 1439-1449, July 2009, doi: 10.1109/TAC.2009.2019796.

[17]D. L. H. Aik and G. Andersson, “Use of participation factors in modal voltage stability analysis of multi-infeed HVDC systems,” in IEEE Transactions on Power Delivery, vol. 13, no. 1, pp. 203-211, Jan. 1998, doi: 10.1109/61.660879.
[18]M. R. Djalal, A. Imran and I. Robandi, “Optimal placement and tuning power system stabilizer using Participation Factor and Imperialist Competitive Algorithm in 150 kV South of Sulawesi system,” 2015 International Seminar on Intelligent Technology and Its Applications (ISITIA), Surabaya, Indonesia, 2015, pp. 147-152, doi: 10.1109/ISITIA.2015.7219970.
[19]D. Brahma and N. Senroy, “Estimation of Dynamic Grid Flexibility Using Matrix Perturbation Theory,” in IEEE Transactions on Power Systems, vol. 37, no. 3, pp. 2491-2494, May 2022, doi: 10.1109/TPWRS.2022.3155922.
[20]X. Mestre, “Improved Estimation of Eigenvalues and Eigenvectors of Covariance Matrices Using Their Sample Estimates,” in IEEE Transactions on Information Theory, vol. 54, no. 11, pp. 5113-5129, Nov. 2008, doi: 10.1109/TIT.2008.929938.
[21]F. Ruggiero, “The Effect of Radiation Damping and Noise on the Transverse Mode Coupling Instability Due to Localized Structures,” in IEEE Transactions on Nuclear Science, vol. 32, no. 5, pp. 2344-2346, Oct. 1985, doi: 10.1109/TNS.1985.4333907.
[22]L. Yang, X. Xiao, D. Zhang and B. Gao, “Analysis of damping conservation in subsynchronous oscillation,” 2011 IEEE Electrical Power and Energy Conference, Winnipeg, MB, 2011, pp. 357-361, doi: 10.1109/EPEC.2011.6070225.
[23]S. Zhao, X. Chang, R. He, “Borrow damping phenomena and negative damping effect of PSS control,” in PROCEEDINGS-CHINESE SOCIETY OF ELECTRICAL ENGINEERING, vol 24, no. 11, pp. 7-11, May 2004, doi: 10.13334/j.0258-8013.pcsee.2004.05.002.
[24]X. Xiao, L. Yang, D. Zhang, “Analysis on sub-synchronous damping conservation character based on eigenvalue method,” in Power Syst. Technol, vol. 33, no. 11, pp. 80-84, Nov 2011, doi: 10.13335/j.1000-3673.pst.2011.11.017.
[25]P. Kundur, Power System Stability and Control. New York, NY, USA: McGraw-Hill, 1994.
[26]J. Luo, S. Bu, F. Teng, “An Optimal Modal Coordination Strategy based on Modal Superposition Theory to Mitigate Low Frequency Oscillation in FCWG Penetrated Power Systems,” in International Journal of Electrical Power & Energy Systems, vol. 120, Sept. 2020, doi: 10.1016/j.ijepes.2020.105975.
[27]I. Dobson, J. Zhang, S. Greene, H. Engdahl and P. W. Sauer, "Is strong modal resonance a precursor to power system oscillations?," in IEEE Transactions on Circuits and Systems I: Fundamental Theory and Applications, vol. 48, no. 3, pp. 340-349, March 2001, doi: 10.1109/81.915389.
[28]C. Canizares et al., "Benchmark Models for the Analysis and Control of Small-Signal Oscillatory Dynamics in Power Systems," in IEEE Transactions on Power Systems, vol. 32, no. 1, pp. 715-722, Jan. 2017, doi: 10.1109/TPWRS.2016.2561263.

Xianyu Zhou received the B.S. degree in electrical engineering and its automation from North China Electric Power University, Beijing, China, in 2018 and the M.S. degree in electrical engineering from Northeastern University, Shenyang, China, in 2021. She is currently pursuing the Ph.D. degree with the Department of Electrical and Electronic Engineering, The Hong Kong Polytechnic University, Hong Kong SAR, China. Her current research interests include stability analysis of renewable penetrated power systems.

Siqi Bu (S’11-M’12-SM’17) received the Ph.D. degree from the electric power and energy research cluster, The Queen’s University of Belfast, Belfast, U.K., where he continued his postdoctoral research work before entering industry. Then he was with National Grid UK as an experienced UK National Transmission System Planner and Operator. He is an Associate Professor and Associate Head with Department of Electrical and Electronic Engineering, The Hong Kong Polytechnic University, Kowloon, Hong Kong, Associate Director of Research Centre for Grid Modernisation, and a Chartered Engineer with UK Royal Engineering Council, London, U.K.. His research interests include power system stability, operation and economics considering renewable energy integration, smart grid application and transport electrification.

Dr Bu is an Editor of IEEE Transactions on Power Systems, IEEE Transactions on Consumer Electronics, IEEE Power Engineering Letters, IEEE Access, IEEE Open Access Journal of Power and Energy, CSEE Journal of Power and Energy Systems, Protection and Control of Modern Power Systems，Journal of Modern Power Systems and Clean Energy and Advances in Applied Energy. He a Fellow of IET, Chairman of IET HK Power and Energy Section, and Co-Chairman of IET DPSP 2025 and APSCOM 2025.